# Functional analysis and molecular modeling show a preserved wild-type activity of p53$^{C238Y}$

**Marco Ferrone,[1] Federica Perrone,[2] Elena Tamborini,[2] Maria Silvia Paneni,[1] Maurizio Fermeglia,[1] Simona Suardi,[2] Elisa Pastore,[2] Domenico Delia,[3] Marco A. Pierotti,[3] Sabrina Pricl,[1] and Silvana Pilotti[2]**

[1]Molecular Simulation Engineering Laboratory, Department of Chemical Engineering, University of Trieste, Trieste, Italy and [2]Unit of Experimental Molecular Pathology, Department of Pathology, and [3]Department of Experimental Oncology, Istituto Nazionale per lo Studio e la Cura dei Tumori, Milan, Italy

## Abstract

**In human tumors, p53 is often disabled by mutations in its DNA-binding domain and is thus inactive as a transcription factor. Alternatively, *MDM2* gene amplification or up-regulation represents a mechanism of p53 wild-type inactivation, mainly reported in soft tissue sarcomas. In a previous *TP53* analysis carried out on sporadic and NF1-related malignant peripheral nerve sheath tumors, in two cases, we observed the occurrence of C238Y missense mutation, leading to p53 stabilization unexpectedly coupled with immunophenotypic MDM2 overexpression. To investigate this *TP53* missense mutation not yet functionally characterized in mammalian cell, we did *MDM2* Southern blot and p53$^{C238Y}$/MDM2 biochemical and functional analyses followed by molecular modeling. The results showed a lack of *MDM2* gene amplification, evidence of p53-MDM2 protein complexes, and presence of a p53 that retains the ability to become phosphorylated on Ser$^{15}$ and to induce the transcription of p21$^{waf1}$. Additional molecular modeling data highlighted the structural similarities between p53$^{C238Y}$ and wild-type p53, further supporting that the p53$^{C238Y}$ mutant still retains functional wild-type p53 properties. [Mol Cancer Ther 2006;5(6):1467–73]**

## Introduction

*TP53* is the most frequently mutated gene in human cancers, and its regulation, such as its pattern of actions, is wide and not totally fully investigated. Many physiologic functions are checked by p53 through transcriptional regulation of its downstream genes by binding to specific genomic sites as a tetramer. The activity of p53 is mainly positively regulated by p14$^{ARF}$ and negatively by MDM2 (1). The major action of MDM2 on p53 is exerted through its E3 ligase ubiquitination activity that blocks the p53 transcriptional function, promoting its nuclear export, and provides a signal for p53 degradation (2).

In malignant tumors, *TP53* missense mutations are thought to be dominant, preferentially affecting highly conserved amino acids and located near the DNA-binding surface of the protein, which, being trascriptionally inactive, is unable to induce MDM2 and thus to be degraded. Moreover, p53-mediated transactivation may be also inhibited by an aberrant p53-MDM2 interaction due to an up-regulation of *MDM2* gene, which shuts down p53 functionality. Gene amplification represents the main mechanism of MDM2 overexpression, and the highest frequency of *MDM2* amplification is observed in soft tissue tumors (3), including liposarcoma (4), and malignant peripheral nerve sheath tumors (MPNST; ref. 5). Simultaneous *TP53* mutation and *MDM2* amplification do not generally occur within the same soft tissue tumor, suggesting that *MDM2* amplification is an alternative effective means for p53 inactivation (5). Immunophenotipically, on surgical specimen, p53 inactivation by missense mutations leads to a p53 stabilization and overexpression with a strong nuclear decoration in 50% to 90% of the tumoral cell, whereas, in a quite mutually exclusive fashion, the *MDM2* amplification correlates with a p53$^{+}$/MDM2$^{+}$ immunophenotype coupled with a wild-type (wt) *TP53* genotype (4).

In a previous *TP53* analysis carried out on sporadic and NF1-related MPNST, we observed the occurrence of the TAT→TGT missense mutation at codon 238 in exon 7, responsible for Cys to Tyr substitution in two sporadic cases (6). This mutation has been already reported but not yet functionally investigated in mammalian cells. Unexpectedly, this missense mutation leading to p53 stabilization correlated with immunophenotypic MDM2 overexpression in both MPNSTs. To explain the unpredicted p53$^{+}$/MDM2$^{+}$ immunophenotype in the presence of *TP53* missense mutation, we did *MDM2* Southern blot and p53$^{C238Y}$/MDM2 biochemical and functional analyses followed by molecular modeling.

The results of both functional analysis and molecular modeling point out that p53$^{C238Y}$ still retains functional wt p53 properties.

## Materials and Methods

### Patients, Tissues, and Results of Previously Done Immunophenotypic and Molecular Analyses

Patient 1 was a 37-year-old male diagnosed with sporadic MPNST of the right leg treated with a wide surgical

Received 1/9/06; revised 4/6/06; accepted 4/27/06.

**Grant support:** Italian Association for Cancer Research.

The costs of publication of this article were defrayed in part by the payment of page charges. This article must therefore be hereby marked advertisement in accordance with 18 U.S.C. Section 1734 solely to indicate this fact.

**Requests for reprints:** Sabrina Pricl, Molecular Simulation Engineering Laboratory, Department of Chemical Engineering, University of Trieste, Piazzale Europa 1, 34127 Trieste, Italy. Phone: 39-40-5583750; Fax: 39-40-569823. E-mail: sabrina.pricl@dicamp.units.it



doi:10.1158/1535-7163.MCT-06-0012

excision. Grossly, the tumor involved the tibial nerve and, microscopically, showed pure epithelioid growth coupled with strong S-100 protein immunoreactivity, features supporting the diagnosis of epithelioid variant MPNST. Two years later, the patient presented bilateral pulmonary metastases treated by surgery followed by radiotherapy and chemotherapy. He died of disease 44 months after disease onset.

Patient 2 was a 55-year-old female who 40 years before was treated by radiotherapy for a non–Hodgkin's lymphoma not otherwise specified of the left maxillary region elsewhere. She presented a 7-cm, deep-seated, circumscribed, left submandibular mass with a fleshy consistency. Grossly, the tumor involved the hypoglossal nerve and, microscopically, showed epithelioid areas in addition to spindle-cell elements identical to that of conventional sporadic MPNST. A wide surgical excision was done; however, because no cleaning of the margins was achieved, radiotherapy and chemotherapy were planned, which were administered elsewhere.

Immunoperoxidase immunophenotyping, done with antibodies against p53 (DO7, YLEM, Rome, Italy) and MDM2 (IF2, Oncogene Science, San Diego, CA), showed nuclear positivity for both markers in each case (6).

Mutational analysis for the most frequently affected exons (from 5 to 8) of the *TP53* gene was done on formalin-fixed paraffin-embedded tissues by nested PCR-single-strand conformational polymorphism and direct automated DNA sequencing. It revealed the presence of the same type of missense mutation at codon 238, TGT versus TAT, responsible for the amino acidic substitution Cys to Tyr (6) in both patients.

In addition, the analysis of the *9p21* locus indicated homozygous deletion of *p16$^{INK4a}$*, *p14$^{ARF}$*, and *p15$^{INK4b}$* in case 1 and loss of *p16$^{INK4a}$* in case 2 (6, 7).

### Molecular Analysis

Southern blotting analysis for *MDM2* gene amplification was done as described previously (4). DNA (7 μg) was digested with *Eco*RI and separated on 0.7% agarose gel. Filter blot was sequentially hybridized with a $^{32}$P-radiolabeled human *MDM2* cDNA probe and a control probe (β-globin) to verify an equal sample loading.

### Biochemical Analysis

Coimmunoprecipitation experiments and Western blotting analyses for p53-MDM2 complexes were done on tumor frozen specimens as described elsewhere (8).

### Site-Specific Mutagenesis

Site-specific mutagenesis was done using the Promega kit (Promega, Madison, WI) following the manufacturer's instructions. The mutation was introduced into a mammalian wt p53-expressing vector using the following primer: 5′-ACAACTACATGTATAACAGTTCCTG-3′. To verify exact introduction of the point mutation in the p53 vector, the plasmid DNA was subjected to automated DNA sequencing (377 DNA Sequencer, ABI PRISM-PE, Applied Biosystems, Foster City, CA), following standard protocols.

### Functional Characterization of p53$^{C238Y}$

Transient transfections of SAOS2 cells with pcDNA3 expression constructs coding for p53$^{WT}$ or p53$^{C238Y}$ were done with LipofectAMINE 2000 (Invitrogen, Carlsbad, CA). An empty pcDNA3 was used for mock transfections. Cells were harvested 72 hours after transfection, and extracts were analyzed by immunoblotting with monoclonal antibodies specific for total p53 (DO7, DAKO, Carpinteria, CA), p21$^{waf1}$ (Lab Vision Corp., Freemont, CA), p53 phosphorylated Ser$^{15}$ (Cell Signal Technology, Beverly, MA), and β-actin (Sigma, St. Louis, MO). Binding of antibodies was revealed by enhanced chemiluminescence (Amersham, Little Chalfont Buckinghamshire, England).

### Molecular Modeling

All molecular dynamics simulations were carried out by using the *Sander* module within the AMBER 7 suite of programs (9) and the *parm94* all-atom force field by Cornell et al. (10); further computational details are available as Supplementary Material. Surface areas were estimated with the MSMS software package (11). The high-resolution crystallographic coordinates of p53 core domain (chain B, 1TUP.pdb; ref. 12) were used as starting geometry for both wt and mutant proteins. The C238Y mutation was introduced into the wt p53 structure using the Biopolymer module of Insight II (version 2001, Accerlys, Inc., San Diego, CA) by swapping the mutant residue into the specific site (13). The appropriate tyrosine rotamer was chosen according to a validated procedure (14). All molecular dynamics simulations were run with explicit water (15) and counterions, using periodic boundary conditions, and the particle mesh Ewald approach (16) to introduce long-range electrostatic effects. The relative stability of the p53 wt and p53$^{C238T}$ proteins was evaluated in terms of free energy of the relevant systems by post-processing the molecular dynamics trajectories with the molecular mechanics/Poisson-Boltzmann surface area (MM/PBSA) technique (17). Accordingly, the free energy $\Delta G_{tot}$ of a protein in solution is calculated as the sum of the molecular mechanical ($E_{MM}$) energies of the solute, solvation free energies ($\Delta G_{solv}$) as approximated by continuum models, and the solute entropy variation (−TS):

$$\Delta G_{tot} \approx E_{MM} + \Delta G_{solv} - TS_{MM} = E_{MM} + \Delta G_{PB} + \Delta G_{NP} - TS_{MM} \quad (A)$$

where

$$E_{MM} = E_{int} + E_{vdW} + E_{coul} \quad (B)$$

$E_{int}$ represents the internal strain in the molecule, $E_{vdW}$ the van der Waals attraction or repulsion, and $E_{coul}$ the electrostatic interactions. In Eq. A, the difference of $E_{MM} - TS_{MM}$ represents the unsolvated free energy of the solute, whereas the free energy of solvation is given by the sum $\Delta G_{PB} + \Delta G_{NP}$. $\Delta G_{NP}$ is the nonpolar solvation energy (i.e., the energy to form a cavity in the solvent along with the solute-solvent van der Waals interactions), which we take to be a liner function of the solvent-accessible

surface area (SASA): $\Delta G_{NP} = \gamma$ (SASA) + $\beta$, in which $\gamma$ = 0.00542 kcal/Å$^2$, $\beta$ = 0.92 kcal/mol, and SASA is the solvent-accessible molecular surface. $\Delta G_{PB}$ is the electrostatic contribution to the solvation energy, determined by numerically solving the linearized Poisson-Boltzmann equations (18, 19), using the iterative finite-difference method implemented in the DelPhi software package (20). The protein entropy of each molecular dynamics snapshot structure was estimated by harmonic normal mode analysis (21) using the *nmode* module of AMBER.

Finally, a preliminary three-dimensional model structure of the full-length p53 protein was built by a combination of homology-based techniques (22). The quality of the model was assessed by using different validation tools (23, 24). Ramachandran plot statistics indicated that 93% of the main-chain dihedral angles were found in the most favorable region, thus confirming the quality of the preliminary three-dimensional model of full-length human p53 protein. Moreover, the secondary structure content of the three-dimensional full-length p53 protein model (13% α-helix, 25% β-sheet, and 62% coil) is in perfect agreement with the secondary structure content experimentally determined on different p53 constructs (25).

## Results

### Molecular Analysis

Southern blotting analysis was done on MPNST of which frozen material was available (patient 2) to investigate the mechanism responsible for MDM2 overexpression detected by immunohistochemistry and described previously (6). As shown in Fig. 1A, a band of 4 kb corresponding to *MDM2* gene was observed in MPNST but with intensity comparable with the negative control (normal lymphoblastoid cell line). In the positive control, a well-differentiated liposarcoma, *MDM2* resulted to be, at least, 10 times more expressed. We concluded that no *MDM2* gene amplification was present in the MPNST.

### Biochemical Analysis

To verify the p53-MDM2 protein complex formation in sporadic MPNST showing p53$^+$/MDM2$^+$ immunophenotype associated to C238Y *TP53* genotype, nuclear protein extracts from patient 2 tumor were immunoprecipitated using a specific α-p53 monoclonal antibody. The subsequent Western blot with a polyclonal p53 antibody allowed us to observe a band of 50 kDa in MPNST and in the positive control used in the experiment (well-differentiated liposarcoma). After stripping the membrane and incubation with an α-MDM2 antibody, a band of 90 kDa was observed in the same lane (Fig. 1B), indicating a p53 and MDM2 physical interaction.

### Functional Analyses of p53$^{C238Y}$

The p53$^{C238Y}$ was analyzed in transient transfection experiments in the p53-null SAOS2 cells for its ability to become phosphorylated on Ser$^{15}$, a residue targeted by ATM, and to induce the transcription of p21$^{waf1}$. Like wt p53, p53$^{C238Y}$ underwent phosphorylation on Ser$^{15}$, and more significantly, it induced the expression of p21$^{waf1}$ protein (Fig. 1C). In similar tests, other p53 mutants, such as the p53$^{175H}$ and p53$^{282G}$, were not phosphorylated on Ser$^{15}$ and unable to transactivate p21$^{waf1}$ (data not shown). Thus, the functional activity of p53$^{C238Y}$ is preserved, at least for the properties we have examined.

### Molecular Modeling

Human p53 has 10 cysteine residues, all of which, interestingly, are located within the DNA-binding domain. These residues seem to gather in two clusters: one cluster (Cys$^{176}$, Cys$^{238}$, and Cys$^{242}$, along with H179) binds to the $Zn^{2+}$ ion, which stabilizes the loop/helical structure of the protein core domain, and the other cluster (Cys$^{124}$, Cys$^{135}$, Cys$^{141}$, Cys$^{275}$, and Cys$^{277}$) is in the β-sheet and/or loop-sheet-helix region. Mutations of these cysteines are rare in

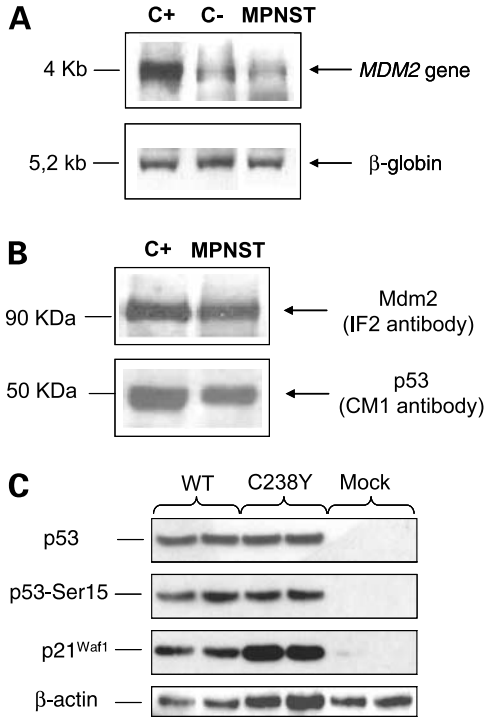


**Figure 1.** Molecular, biochemical, and functional analysis of C238Y. **A,** Southern blot analysis of *Eco*RI-digested DNA from MPNST carrying C238Y mutation (patient 2) and from normal lymphoblastoid cell line and a well-differentiated liposarcoma used as negative and positive controls, respectively. A 258-bp fragment spanning exons 2 and 3 of the *MDM2* gene was used as probe. The *MDM2* gene amplification was seen in the positive control, whereas MPNST showed a MDM2 band (4 kb) with intensity comparable with the negative control. Southern blot with β-globin probe showed equal DNA loading of the lanes. *C+*, positive control; *C−*, negative control. **B,** coimmunoprecipitation experiments and Western blotting analyses for p53-MDM2 complexes on MPNST carrying C238Y mutation (patient 2). Nuclear protein extracts were immunoprecipitated using a specific α-p53 monoclonal antibody. The subsequent Western blot with a polyclonal p53 antibody (CM1) revealed a band of 50 kDa in MPNST and in the well-differentiated liposarcoma, used as positive control. After stripping the membrane and incubation with an α-MDM2 antibody (IF2), a band of 90 kDa was observed in MPNST, indicating a p53 and MDM2 physical interaction. **C,** immunoblot analysis done on total cell extracts from SAOS2 transiently transfected with constructs carrying the wt or C238Y mutant form of p53. Mock transfections were done with an empty plasmids. Protein loading per lane was verified by reprobing membranes for β-actin. Duplicate experiments.

human cancers; however, there has been an interest in redox modulation of p53 by these cysteine clusters (26–30). Thus, the mutated amino acid considered in this work, $Cys^{238}$, is a zinc-binding residue, and its mutation to a serine residue in earlier studied (27) was found to abolish the DNA-binding function of p53. Therefore, in the light of this information and to get an insight into the nature of the possible structural perturbation induced by the mutation C238Y in the core domain of p53, 1-ns-unrestrained molecular dynamics simulations on both wt and mutant protein was computed in the presence of explicit solvent and counterions. The structural results obtained from the 1-ns molecular dynamics runs are worthy to comment and are given in Fig. 2A and B and Table 1. The overall root-mean-square deviation between the wt and the mutant p53 is below 1.4 Å, which indicates the existence of minimal structural differences between the two proteins. The structure of the region in the vicinity of the mutation site is the most influenced by the residue substitution, as expected, albeit the relevant root-mean-square deviation is only 1.63 Å. Indeed, the replacement of the aliphatic cysteine chain with the bulkier aromatic ring of tyrosine results in an estimated increase of the residue nonpolar surface area of 106 $Å^2$, which contributes to more extensive, favorable hydrophobic interaction with residues around position 238, which is well buried within the protein interior. At the same time, the corresponding estimated increase in the molecular surface area and volume due to

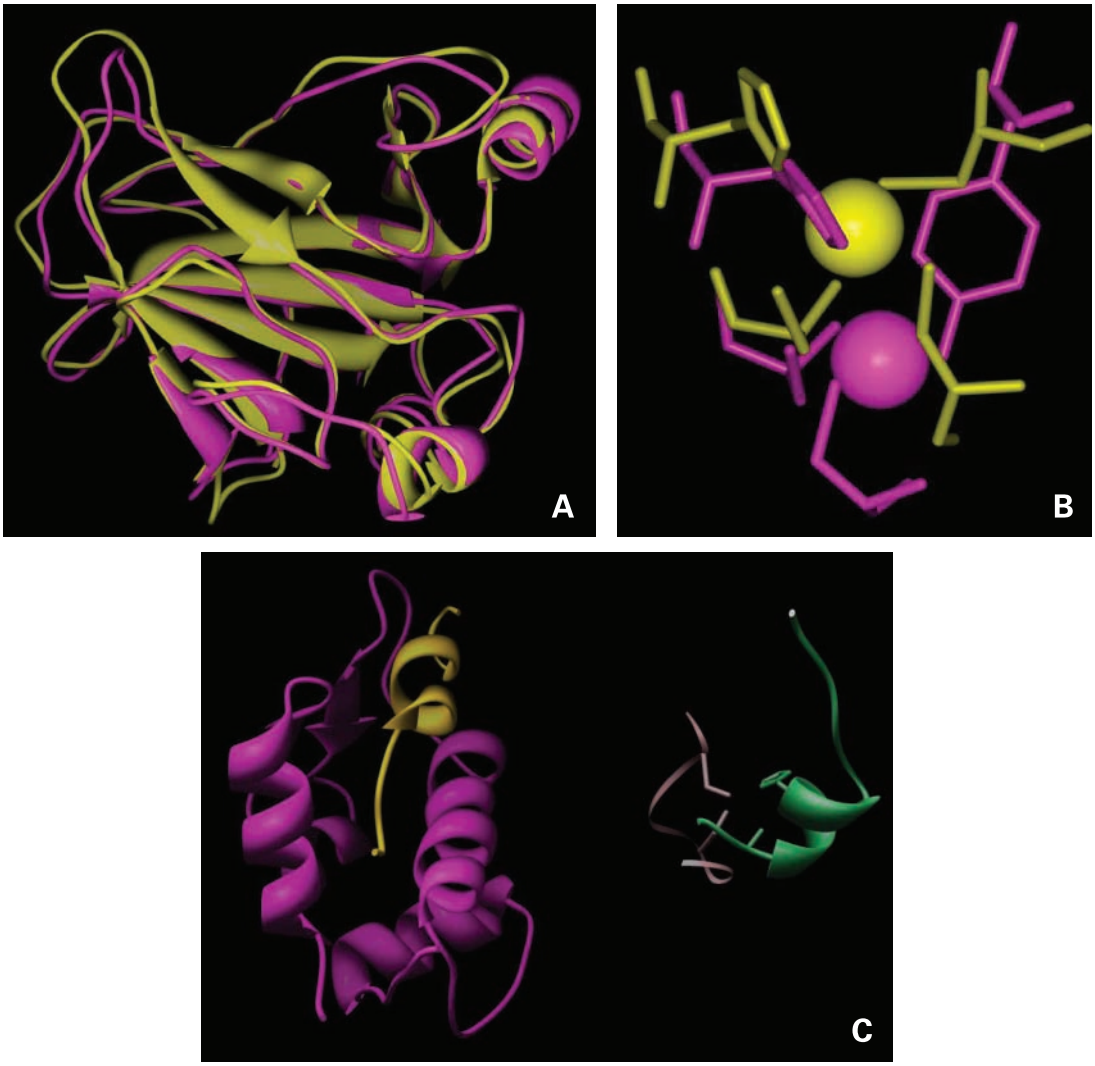


**Figure 2.** **A,** superimposed molecular dynamics equilibrated peptide backbone atoms of the core domain of the wt (*yellow ribbon*) and C238Y mutant (*purple ribbon*) of p53. **B,** conformational overlap of the residues of L2 and L3 loops of wt (*yellow sticks*) and C238Y mutant (*purple sticks*) forms of p53 coordinating the $Zn^{2+}$ ion (*ball representation*). *Top left,* H179; *bottom left,* C176; *top right,* C/Y238; *bottom right,* C242. **C,** relative position of the zinc-binding residues (*pink* and *light green ribbons*) and p53 transactivation domain (*gold ribbon*) in the three-dimensional full-length p53 model. *Purple ribbon,* MDM2 protein docked onto the p53 sequence. Hydrogen atoms are omitted for clarity.

**Table 1. Structural comparison of wt p53 with the C238Y mutant**

| Structure superposition mode* | Number of superimposed atoms | RMSD† (Å) |
|---|---|---|
| p53 DNA-binding region (residues 96–289) | 1,552 | 1.32 |
| p53 loops L2 and L3 (residues 163–195 and 236–251) | 392 | 1.49 |
| p53 residues within 5 Å distance from the zinc atom | 96 | 1.63 |
| p53 residues coordinating the zinc atom | 32 | 1.44 |

*Superimposed peptide backbone atoms.
†RMSD, root-mean-square deviation, defined as $\mathrm{RMSD} = [(1/N)\Sigma_i(r_i - r_{i,\mathrm{ref}})^2]^{1/2}$ where $\Delta r_i = r_i - r_{i,\mathrm{ref}}$ is the atomic displacement vector of atom $i$.

the mutation (45 Å$^2$ and 30 Å$^3$, respectively) results in higher exchange repulsion in this position. The highly unfavorable energy penalty paid for the burial for the more polar side chain of tyrosine in highly hydrophobic environment is also partly compensated by the positive interactions of the π-electrons of the tyrosine side chain ring with the zinc ion, which stabilize the cation in the proper position. The evidence from molecular dynamics that C238Y is still able to bind zinc is in harmony with the experimental work of Bullock et al. (31), which observed that the tumorigenic mutation at the zinc-binding site C242S, expressed as 20°C, remained bound to zinc during urea denaturation with 1:1 stoichiometry. Finally, the analysis of the molecular dynamics trajectories of both wt and mutant p53 proteins revealed that neither residue at position 238 is involved in direct permanent hydrogen bonding with any neighboring amino acids. In this respect, Bullock et al. (32) have found that for the C242S mutation, which is involved in an important hydrogen bond network with the backbone amides of four loop 3 residues (i.e., G244, G245, M246, and N247) and helps to present R248 for its contacts to the DNA minor groove, the estimated proteins folded at 37°C is ~50%.

The low degree of structural perturbation induced by the mutant residue is supported by further analysis of our molecular dynamics trajectories. As for the wt protein, in the C238Y mutant simulation, the backbone C=O group of the zinc ligand C242 is involved in an alternate hydrogen bond with the NH backbone moieties of N247 [average dynamic length (ADL), 2.85 Å] and G245 (ADL, 2.79 Å), respectively. Further, the backbone amide of C242 makes another stabilizing H-bond with the backbone carbonyl oxygen of N239 (ADL, 3.08 Å). R175, adjacent to the zinc ligand C176, is surrounded by portions of loops 2 and 3 and is involved in interactions bridging the two. In details, the R175 side chain Nε donates an H-bond to the backbone C=O of M237 on the L3 (ADL, 3.01 Å), whereas the Nη1 atom of the guanidinium group is engaged in a similar interaction with the main-chain carbonyl of P191 on L2 (ADL, 2.79 Å) The other nitrogen of the same moiety, Nη2, entails a bifurcated H-bond with the carboxylate oxygen atoms (Oδ1 and Oδ2) of D184 on L2 (ADL, 1.98 Å and 2.28 Å, respectively), which in turn are further stabilized by H-bonding to water molecules 2,230 and 2,221, respectively (ADL, 3.06 Å and 3.04 Å). Accordingly, all these evidences concur to conclude that the structural changes induced by the presence of the tyrosine mutant residue at position 238 of the p53 core domain are sufficiently small to justify the almost native conformation of the $p53^{C238Y}$ protein.

With significant sampling of stabile protein conformations, MM/PBSA allowed us to estimate the free energy difference between the wt and the C238Y mutant p53. Table 2 presents the results of MM/PBSA analysis using 1,000 snapshots (i.e., one every 10 ps) from the wt and the mutant protein trajectories, respectively. As we can see from Table 2, the $\Delta\Delta G_{\mathrm{wt\text{-}mut}} = \Delta G_{\mathrm{tot}}(\mathrm{wt}) - \Delta G_{\mathrm{tot}}(\mathrm{mut}) = 3.23$ kcal/mol favors the mutant. In fact, we must recall that a negative number in $\Delta\Delta G_{\mathrm{wt\text{-}mut}}$ means an unfavorable substitution, whereas a positive $\Delta\Delta G_{\mathrm{wt\text{-}mut}}$ indicates the preference for the given residue at the mutated position. Interestingly, from the inspection of the C238Y p53 mutant molecular dynamics trajectory, we observe that the Y238 -OH side chain group is involved in a stable, persistent intermolecular hydrogen bond with water 2,037, characterized by an ADL, 2.82 Å. The same water molecule forms another hydrogen bond with the NH backbone moiety of M246 (ADL, 2.39 Å). The results shows that the presence of this hydrogen bond, clearly absent in the C238 wt protein, makes a substantial contribution to the mutant protein stability. In this respect, our present guess is that the stability increase calculated for the C238Y variant may be due to the fact that the loop anchored by the water-mediated H-bridge, comprising residues from S241 to N247, is less flexible in the mutant than in the wt protein. Finally, we can add that the $\Delta\Delta G_{\mathrm{wt\text{-}mut}}$ value obtained is in sound agreement with previous experimental results

**Table 2. MM/PBSA energies (and SDs) calculated for the wt and C238Y p53 mutant**

| Energy components | Wt | C238Y |
|---|---|---|
| $E_{\mathrm{coul}}$* | −2,498.32 (15.41) | −2,584.75 (14.22) |
| $E_{\mathrm{vdW}}$* | −336.69 (2.13) | −331.01 (1.99) |
| $E_{\mathrm{int}}$* | 1,497.67 (11.55) | 1,502.01 (12.00) |
| $E_{\mathrm{MM}}$* | −1,337.34 (16.01) | −1,413.75 (16.87) |
| $-TS_{\mathrm{MM}}$* | −1,044.81 | −1,041.93 |
| $E_{\mathrm{MM}} - TS_{\mathrm{MM}}$ | −2,382.15 | −2,455.68 |
| $\Delta G_{\mathrm{PB}}$* | −1,579.06 (24.65) | −1,509.27 (20.21) |
| $\Delta G_{\mathrm{NP}}$* | 32.15 (0.41) | 32.66 (0.52) |
| $\Delta G_{\mathrm{tot}}$ | −3,929.06 (13.73) | −3,932.29 (13.99) |
| $\Delta\Delta G_{\mathrm{wt\text{-}mut}}$ | 3.23 | — |

NOTE: Mean energies are averaged >1,000 snapshots (one every 10 ps). SDs are of 50 batched means, each averaged >20 snapshots (200 ps of trajectory). All units are in kcal/mol. For the entropy terms, $T$ is taken to be 298 K. As defined in the text, MM/PBSA is a combined molecular mechanical, Poisson-Boltzmann, and surface-area model used to estimate free energy.
*Energy components are as defined in Eqs. A and B.

obtained on different proteins, where different amino acids have been replaced by tyrosine residues (33).

Lastly, the inspection of the three-dimensional model of the full-length p53 reveals that the site of mutation is quite far from the transactivation domain (Fig. 2C). Therefore, the minimum, local structural alteration induced by the presence of the mutant residue Y238 should not interfere with the MDM2 binding, in harmony with our experimental finding.

## Discussion

To explain the unexpected p53$^{+}$/MDM2$^{+}$ immunophenotype in the presence of the missense C238Y *TP53* mutation observed in two sporadic MPNSTs, we did *MDM2* molecular and p53$^{C238Y}$/MDM2 biochemical analyses on frozen MPNST specimens and p53$^{C238Y}$ functional analyses on the p53-null SAOS2 cells. The analysis results showed lacking of *MDM2* gene amplification, evidence of p53-MDM2 protein complexes, and presence of a p53 that retains the ability to become phosphorylated on Ser$^{15}$ and to induce the transcription of p21$^{waf1}$.

Because all these findings spoke in favors of the presence of a mutated p53 with wt functional characteristics, we further investigated the wt functionality of p53$^{C238Y}$ by molecular modeling, which, through extensive molecular dynamics simulations, highlighted the structural similarities between p53$^{C238Y}$ and wt p53. Indeed, the presence of the mutant residue did not result in a substantial modification of the native conformation of the protein: the phenyl ring of the tyrosine residue could be accommodated in the binding site without sterical incompatibilities stabilizing the zinc ion in place. Further, the surrounding residues did not result strongly affected by this substitution, and the important structural stabilizing interactions, in which they were involved in the wt protein, were still all present in the molecular dynamics trajectory of the mutant protein. As the relative stability of the two proteins is concerned, the application of the MM/PBSA computational technique suggests that the mutant protein is more stable than the wt by 3.23 kcal/mol. Keeping in mind that these calculations were not applied to the entire p53 protein but only to its core domain, this conclusion, although in line with our experimental evidences, should be taken as a preliminary result, and further biochemical studies as well as molecular simulations are clearly needed to finally support these evidences. The inspection of the relevant molecular dynamics trajectory revealed the presence of a water-mediated H-bond between *Y238* and *M246*, which lowing the flexibility of the loop encompassing residues 241 and 247, increased the mutant protein stability.

Finally, an inspection of the preliminary three-dimensional model of the full-length p53 revealed that the 238 residue is spatially far from the MDM2 transactivation sequence. This observation, coupled with the overall preserved protein conformation in the presence of the C238Y mutation, allowed us to conclude that the physical interaction of MDM2 with p53 should not be affected in the mutant protein, in harmony with our evidence of p53-MDM2 protein complex formation. Cumulatively, the evidence resulting from the unrestrained molecular dynamics simulation done on both p53 wt and p53$^{C238Y}$ concurred to confirm that the presence of the C238Y mutation in the core domain of p53 does not result in global structural changes in the mutant protein. This is, at our knowledge, the first description of functional/structural properties of this p53 missense mutation.

### Acknowledgments

We thank Enrico Fontanella for technical assistance.

### References

1. Harris SL, Levine AJ. The p53 pathway: positive and negative feedback loops. Oncogene 2005;24:2899 – 908.

2. Freedman DA, Levine AJ. Nuclear export is required for degradation of endogenous p53 by MDM2 and human papillomavirus E6. Mol Cell Biol 1998;18:7288 – 93.

3. Cordon-Cardo C, Latres E, Drobnjak N, et al. Molecular abnormalities of mdm2 and p53 genes in adult soft tissue sarcomas. Cancer Res 1994;54:794 – 9.

4. Pilotti S, Della Torre G, Lavarino C, et al. Distinct mdm2/p53 expression patterns in liposarcoma subgroups: implications for different pathogenetic mechanisms. J Pathol 1997;181:14 – 24.

5. Momand J, Jung D, Wilcynski S, Nilan J. The MDM2 gene amplification database. Nucleic Acids Res 1998;26:3453 – 9.

6. Birindelli S, Perrone F, Oggionni M, et al. Rb and TP53 pathway alterations in sporadic and NF1-related malignant peripheral nerve sheath tumors. Lab Invest 2001;81:833 – 44.

7. Perrone F, Tabano S, Colombo F, et al. p15$^{INK4b}$, p14$^{ARF}$, and p16$^{INK4a}$ inactivation in sporadic and neurofibromatosis type 1-related malignant peripheral nerve sheath tumors. Clin Cancer Res 2003;9:4132 – 8.

8. Butò S, Pierotti MA, Tamborini E, et al. Biochemical uncovering of mdm2/p53 complexes in liposarcomas parallels their immunohistochemical detection. Diagn Mol Pathol 1999;8:125 – 30.

9. Case DA, Pearlman DA, Caldwell JW, et al. AMBER 7. San Francisco (CA): University of California; 2000.

10. Cornell WD, Cieplak P, Bayly CI, et al. A second generation force field for the simulation of proteins and nucleic acids. J Am Chem Soc 1995;117:5179 – 97.

11. Sanner MF, Olson AJ, Spehner JC. Reduced surface: an efficient way to compute molecular surfaces. Biopolymers 1996;38:305 – 20.

12. Cho Y, Gorina S, Jeffrey PD, Pavletich NP. Crystal structure of a p53 tumor suppressor-DNA complex: understanding tumorigenic mutations. Science 1994;265:346 – 65.

13. Reyes CM, Kollman PA. Investigating the binding specificity of U1A-RNA by computational mutagenesis. J Mol Biol 2000;295:1 – 6.

14. Pricl S, Fermeglia M, Ferrone M, Tamborini E. T315I-mutated Bcr-Abl in chronic myeloid leucemia and imatinib: insights from a computational study. Mol Cancer Ther 2005;4:1167 – 74.

15. Jorgensen WL, Chandrasekhar J, Madura JD, Impey RW, Klein ML. Comparison of simple potential functions for simulating liquid water. J Chem Phys 1983;79:926 – 35.

16. Darden T, York D, Pedersen L. Particle mesh Ewald—an Nlog(N) method for Ewald sums in large systems. J Chem Phys 1993;98:1089 – 92.

17. Srinivasan J, Cheathem TE III, Cieplak P, Kollman PA, Case DA. Continuum solvent studies of the stability of DNA, RNA, and phosphoramidate-DNA helices. J Am Chem Soc 1998;120:9401 – 9.

18. Gilson MK, Sharp KA, Honig B. Calculating the electrostatic potential of molecules in solution: method and error assessment. J Comput Chem 1987;9:327 – 35.

19. Honig B, Nicholls A. Classical electrostatics in biology and chemistry. Science 1995;268:1144 – 9.

20. Sitkoff D, Sharp KA, Honig B. Accurate calculation of hydration free

energies using macroscopic solvent models. J Phys Chem 1994;98: 1978 – 88.

**21.** Brooks BR, Janežič D, Karplus M. Harmonic analysis of large systems. 1. Methodology. J Comput Chem 1995;16:1522 – 42.

**22.** Marti-Renom MA, Stuart A, Fiser A, Sánchez R, Melo F, Sali A. Comparative protein structure modeling of genes and genomes. Annu Rev Biophys Biomol Struct 2000;29:291 – 325.

**23.** Laskowski RA, MacArthur MW, Moss DS, Thornton JM. PROCHECK: a program to check the stereochemical quality of protein structures. J Appl Cryst 1993;26:283 – 91.

**24.** Rhodriguez R, Chinea G, Lopez N, Pons T, Vriend G. Homology modeling, model and software evaluation: three related sources. CABIOS 1998;14:523 – 8.

**25.** Bell S, Klein C, Müller L, Hansen S, Buchner J. p53 contains large unstructured regions in its native state. J Mol Biol 2002;322:917 – 27.

**26.** Delphin C, Cahen P, Lawrence JJ, Baudier J. Characterization of baculovirus recombinant wild-type p53. Dimerization of p53 is required for high-affinity DNA binding and cysteine oxidation inhibits p53 DNA binding. Eur J Biochem 1994;223:683 – 92.

**27.** Rainwater R, Parks D, Anderson ME, Tegtmeyer P, Mann K. Role of cysteine residues in regulation of p53 function. Mol Cell Biol 1995;15: 3892 – 903.

**28.** Buzek J, Latonen L, Kurki S, Peltonen K, Laiho M. Redox state of tumor suppressor p53 regulates its sequence-specific DNA binding in DNA-damaged cells by cysteine 277. Nucleic Acids Res 2002;30:2340 – 8.

**29.** Sun XZ, Vinci C, Makmura L, et al. Formation of disulfide bond in p53 correlates with inhibition of DNA binding and tetramerization. Antioxid Redox Signal 2003;5:655 – 65.

**30.** Pivonkova H, Brazdova M, Kasparkova J, Brabec V, Fojta M. Recognition of cisplatin-damaged DNA by p53 protein: critical role of the p53 C-terminal domain. Biochem Biophys Res Commun 2006;339: 477 – 84.

**31.** Bullock AN, Henckel J, DeDecker BS, et al. Thermodynamic stability of wild-type and mutant p53 core domain. Proc Natl Acad Sci U S A 1997; 94:14338 – 42.

**32.** Bullock AN, Henckel J, Fersht AR. Quantitative analysis of residual folding and DNA binding in mutant p53 core domain: definition of mutant states for rescue in cancer therapy. Oncogene 2000;19:1245 – 56.

**33.** Pace CN, Horn G, Herbert EJ, et al. Tyrosine hydrogen bends make a large contribution to protein stability. J Mol Biol 2001;321:393 – 404.